Journal of Electronic Materials (2023) 52:7897–7906
https://doi.org/10.1007/s11664-023-10750-x

ORIGINAL RESEARCH ARTICLE

Low-Cost Layered Double Hydroxides as Inorganic Hole Transport Layer for Perovskite Solar Cells

Xiangsen Ye[1] · Xiaoqing Cao[1] · Lingwei Kong[1] · Xinrui Wang[2] · Rui Zhang[1] · Wenying Shi[1] · Chao Lu[1]

Received: 26 April 2023 / Accepted: 22 September 2023 / Published online: 6 October 2023

Abstract

Perovskite solar cells (PSCs) are expected to be comparable to silicon-based solar cells. However, the high efficiency of PSCs relies on expensive and unstable organics as a hole transport layer (HTL). Here, inorganic layered double hydroxides (LDHs) are chosen as the HTL. LDHs can be better dispersed in organic solvents due to rich hydroxyl groups, conducive to improving PSC quality. Importantly, the LDH layer can perform energy level matching between the perovskite layer and the carbon electrode to improve the hole extraction efficiency and reduce the recombination of electrons and holes. The above synergistic effect of LDHs makes the efficiency of the all-air treated carbon-based PSCs prepared using LDH as HTL achieve champion efficiency of 10.7%. Although the value is not so high, the simple preparation process and low cost confirm LDH as a potential alternative to expensive organic HTLs in the commercialization of PSC.

Xiangsen Ye and Xiaoqing Cao have contributed equally to this work.

✉ Rui Zhang
zhangrui1@mail.buct.edu.cn

✉ Wenying Shi
shiwy@mail.buct.edu.cn

[1] State Key Laboratory of Chemical Resource Engineering, Beijing University of Chemical Technology, 15 Beisanhuan East Road, PO. Box 98, Beijing 100029, People's Republic of China

[2] Key Laboratory of Cosmetic, China National Light Industry, College of Chemistry and Materials Engineering, Beijing Technology and Business University, Beijing 100048, People's Republic of China

Graphical Abstract

We introduced layered double hydroxides as a hole transport layer into carbon-based perovskite solar cells, which have improved power conversion efficiency and stability.

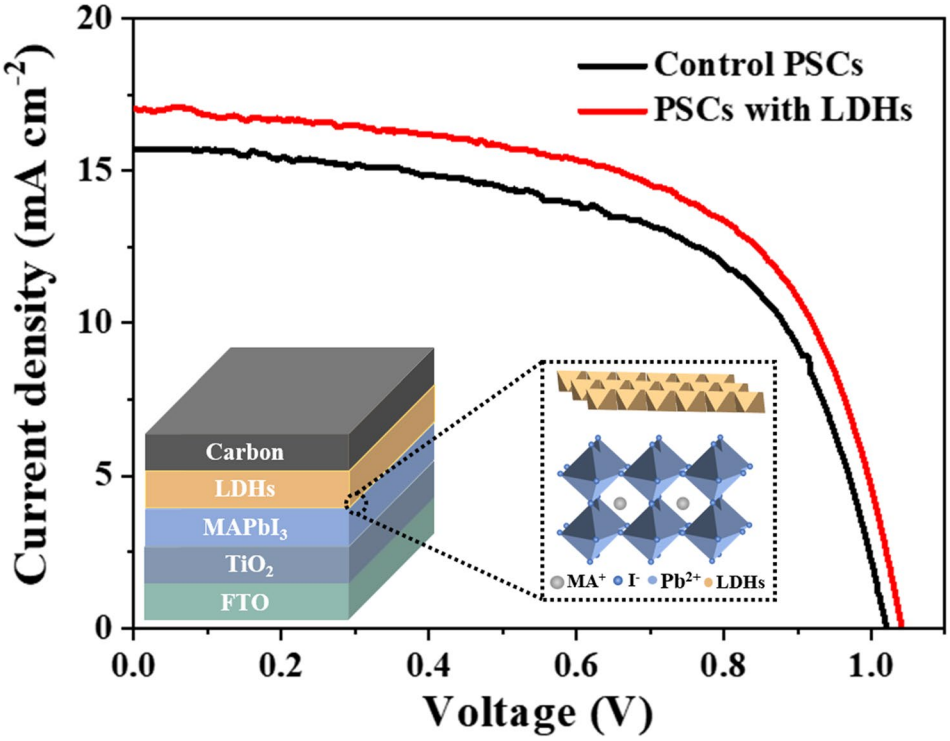

Keywords Perovskite solar cells · layered double hydroxides · hole transport layer · stability · carbon electrode

Introduction

Perovskite solar cells (PSCs) have good photophysical performance, low fabrication cost and high power conversion efficiency (PCE), and are considered as a promising alternative to silicon-based solar cells.[1–5] In recent years, PSCs have developed rapidly, and PCE has increased from 3.8% in 2009 to over 25% currently.[6,7] One of the ways to achieve high PCE with PSCs is to introduce a hole transport layer (HTL) in the device, which can extract photogenerated holes and transport them from the perovskite (PVK) layer to the back contact electrode, thus effectively reducing the charge recombination at the interface and enhancing device performance.[8–11] Currently, the most widely used HTL is the small-molecule 2,2′,7,7′-tetrakis(*N,N*-bis(*p*-methoxyphenyl)amino)−9,9′-spirobifluorene (Spiro-OMeTAD).[12–16] However, the cost of organic HTLs is high because of the complex synthesis process, and organic HTLs also have the disadvantage of poor stability.[17–20] The high cost of Spiro-OMeTAD limits its large-scale application.[10,21] Therefore, it is important to explore inorganic HTLs with low cost and high stability to improve the efficiency and performance of the devices, so as to promote the commercialization of PSCs.

Layered materials have been widely studied and applied due to their excellent electrical, mechanical and chemical properties. Transitional metal dichalcogenides, black phosphorus, boron nitrides, and other layered materials have been widely used in PSCs, and these materials are reliable and effective in achieving higher efficiency and stability.[22,23] Layered double hydroxides (LDHs) are composed of an inorganic layered structure, which possess high stability (heat, moisture and light).[24,25] In this respect, LDH is more suitable for serving as a protective layer for a PVK absorber, preventing moisture and oxygen penetration and improving the stability of PSC devices more effectively than organic materials. LDHs are a class of inorganic functional materials with a layered structure, with variable elemental species and compositional ratios of the main laminates. Importantly, the bandgap of LDHs can be adjusted compared to other HTL materials. The bandgap of LDHs is tunable by adjusting the composition of metal cations

between LDH laminates, which is important in achieving a bandgap match with PVK.[26,27] In addition, LDHs can provide more active sites, reduce the energy barrier, and promote the rapid separation and transport of holes, thus inhibiting the recombination of photo-generated carriers.[28] Therefore, LDHs have the potential to be used as HTL for PSCs. It should be pointed out that the preparation of HTL materials has been very difficult up to now, and LDHs can be easily and economically synthesized, which provides greater advantages in this respect.[29–31] These features indicate that LDHs as HTL materials not only can improve the efficiency of PSCs, but also can reduce the fabrication cost of devices.

In our previous work, inorganic layered double hydroxide nanosheets (LDHs-NS) were introduced into PVK solution, where the microscopic and macroscopic anisotropy of the LDHs-NS guided the anisotropic growth of the PVK crystals.[32] The crystal quality of the PVK films was greatly improved, and the PCE and stability of the devices were enhanced. However, from the perspective of the preparation process, the preparation of nanosheets is relatively complex. Therefore, the starting point of this work is to simplify the experimental preparation process, and further reduce the production cost, laying the foundation for the large-scale introduction of batteries in the future. Here, the MgAl-LDHs were prepared by co-precipitation and used as the HTL in carbon-based PSCs, which has the following advantages. Firstly, LDHs reduce the recombination of carriers at the PSC interface. The valence band of LDH is matched with the PVK valence band, which can transport holes well. Meanwhile, it has a high conduction band bottom, which can better limit the movement of electrons to the anode. Secondly, LDHs have surface hydroxyl groups, so they are well dispersed in organic solvents and evenly spread on the surface of the PVK layer, resulting in good quality of the prepared devices; moreover, the hydroxyl groups combine with the uncoordinated Pb^{2+}, which fills the holes of the PVK layer and prevents direct contact between the carbon electrode and TiO_2 layer. Thirdly, LDHs protect the PVK layer from direct contact with oxygen and heat in the air, preventing the PVK layer from decomposing. The PSCs using LDHs as HTLs can achieve maximum PCE of 10.70%. Although the efficiency is not as good as values reported previously, we use the cheaper carbon counter electrode, and all device fabrication processes are carried out under the actual ambient air conditions, which reduces the fabrication cost and helps to promote the large-scale commercialization of PSCs.

Experimental Section

Materials

All chemicals used were analytical-reagent grade and were used as received without further purification. Fluorine tin oxide (FTO) substrates (7 Ω sq^{-1}) were purchased from Pilkington. Titanium tetraisopropanolate and dimethyl sulfoxide (DMSO, 99.9%) were purchased from Macklin. Mesoporous TiO_2 (Dyesol, 18 NR-T), PbI_2 (99.99%), and CH_3NH_3I (MAI, 99.5%) were purchased from Xi'an Yuri Solar Co., Ltd. *N*,*N*-Dimethylformamide (DMF, 99.8%) was purchased from J&K Chemical Ltd. Chlorobenzene (CB, 99.5%) was purchased from Aladdin. Carbon paste was purchased from Guangzhou Saidi Technology & Trade Development Co., Ltd. $Mg(NO_3)_2{\cdot}6H_2O$ (99%), $Al(NO_3)_2{\cdot}9H_2O$ (99%), $NaNO_3$ (99%), and NaOH (96%) were purchased from Beijing Chemical Reagent Company.

Preparation of LDHs

The MgAl-LDHs used in this experiment was prepared by the co-precipitation method, and the water used is decarbonized water. The schematic diagram of the preparation of MgAl-LDHs is shown in Fig. S1. First, 0.015 mol $Mg(NO_3)_2{\cdot}6H_2O$ and 0.05 mol $Al(NO_3)_2{\cdot}9H_2O$ (molar ratio 3:1) were dispersed in 200 mL of deionized water while configuring 0.25 M of NaOH solution for backup. Then, 0.02 M of $NaNO_3$ solution was added to a three-necked flask, the metal salt solution and alkali solution were dropped into it, and it was stirred with magnetic force, maintaining a pH of about 10 during the whole process. After the dropwise addition was completed, the solution was left to stand for 2 h and cooled to obtain a white colloidal dispersion. It was washed three times by centrifugation with deionized water and dried into powder at 60°C for 24 h. Subsequently, the powder was dispersed in isopropanol and ultrasonicated for 2 h to obtain MgAl-LDHs of isopropanol solutions.

Device Fabrication

FTO was sonicated in detergent, deionized water, isopropanol and absolute ethanol for 20 min sequentially and dried at 60°C with 2 h. Subsequently, 0.4 M titanium tetraisopropanolate dispersed in ethanol was rotated on clean FTO conductive glass at a spin coating at 1000 rpm for 3 s and 2500 rpm for 30 s, then heated at 125°C for 5 min. Subsequently, mesoporous TiO_2 (weight ratio 1:3.5) diluted in ethanol was rotated at 1000 rpm for 3 s and at 3500 rpm for 30 s to spin coat, and then the coating was sintered at 500°C for 30 min in a muffle furnace. Next, 230.5 mg PbI_2 and 79.5 mg MAI were dissolved in the mixed solution of 360 μL DMF and 36 μL DMSO to prepare the PVK solution. The PVK film was spin-coated on the mesoporous TiO_2 layer by spin coating at 1000 rpm for 10 s and 4000 rpm for 20 s, and heated at 100°C for 10 min. Isopropanol solution of MgAl-LDHs was deposited on the PVK layer by spin coating at 4000 rpm for 30 s, and then heated at 100°C

for 5 min. Finally, the carbon electrode was scraped with carbon paste on the absorber layers and heated to 95°C for 30 min. The control PSC devices were fabricated in the similar way as described above, but MgAl-LDHs solution was not spin-coated on the PVK film, and carbon paste was directly scraped on top. The effective area of each cell was approximately 0.07 cm^2. To be clear, all operations were carried out in air.

Measurements and Characterization

The current density-voltage (*J–V*) characteristics of cell devices were measured on a CHI660E (Chenhua, Shanghai) electrochemical workstation under 100 mW/cm^2 simulated AM 1.5 G irradiation using a solar simulator (CEL-AAAS50, Ceaulight). The light intensity was calibrated by the laser power meter (VLP-2000, RanBond). The UV-Vis absorption spectra were recorded with a Hitachi UV-3900H spectrophotometer (Tokyo, Japan). The Fourier- transform infrared (FTIR) test was performed using a PerkinElmer model 100 FTIR spectrometer (Waltham, MA, USA). X-ray photoelectron spectroscopy (XPS) was carried out using an ESCALAB MKII 250 (Thermo Fisher, USA). Cyclic voltammetry (CV) was carried out with a computer-controlled CHI660E electrochemical workstation (Chenhua, Shanghai). The steady-state photoluminescence (PL) spectra were measured on an FS5 fluorescence spectrophotometer (Edinburgh Instruments, UK). Time-resolved photoluminescence spectra (TRPL) were measured using an Edinburgh Instruments FLS980. Electrochemical impedance spectroscopy (EIS) was carried out using an electrochemical workstation (VersaSTAT, USA). The Nyquist curve was fitted by ZView software. X-ray diffraction (XRD) was performed using a Bruker (Germany) D8 Advance x-ray diffractometer with Cu/Kα radiation (λ = 1.54 Å). Scanning electron microscopy (SEM) measurements were performed by a S-4700 (Hitachi, Japan). Atomic force microscopy (AFM) measurements were tested by a DMFASTSCAN2-SYS (Bruker, Germany).

Results and Discussion

Device Characterization

Photovoltaic Performance

To investigate the change of device performance after LDHs was introduced into the cells, we fabricated PSCs with the structure of FTO/compact TiO_2/mesoporous TiO_2/$MAPbI_3$/LDHs/carbon (Fig. 1a). We prepared the isopropyl alcohol solution of MgAl-LDHs with the concentration of 0.1 mg/mL, which was used as the interface passivation materials. The *J–V* curves of the optimal PSC with and without LDHs (named as control PSCs) under AM 1.5G irradiation with an intensity of 100 mW cm^{-2} was shown in Fig. 1b. Table I shows the detailed photovoltaic performance parameters of open-circuit voltage (V_{OC}), short-circuit photocurrent density (J_{SC}), filling factor (FF) and PCE. The FF can be calculated according to the maximal power point (MPP) of the *J–V* curve as shown in equation:[33,34]

$$FF = \frac{J_{mpp} \times V_{mpp}}{J_{SC} \times V_{OC}} \quad (1)$$

where J_{mpp} and V_{mpp} are the current density and voltage at maximal power point. Then, based on the obtained values of J_{SC}, V_{OC} and FF, PCE is calculated using the following equation:[22,35]

$$PCE = \frac{J_{SC} \times V_{OC} \times FF}{P_{in}} \quad (2)$$

where Pin stands for the incident light irradiance and its standard value is 100 mW cm^2 for AM 1.5G irradiation. PCE is the ratio of the total output power generated by the device to the total optical power provided as the input. The PSC with LDHs had a PCE of 10.70%, V_{OC} of 1.04 V, J_{SC} of 17.00 mA cm^{-2}, and FF of 60.49%, whereas the control PSC achieved a PCE of only 9.60%, V_{OC} of 1.02 V, J_{SC} of 15.71 mA cm^{-2}, and FF of 59.89%. It can be seen that the efficiency of the PSC is improved after the modification of LDHs as the interfacial layer. To demonstrate the repeatability of the PSC with LDHs and control PSC devices, histograms of the PCE statistical distribution are provided. Figure S2 showed that the PCE statistics obey a Gaussian distribution and PSC with LDHs devices have good reproducibility.

The Stability of PSCs

The stability of PSCs is very important in practical application, and thermal stability is one of the important aspects that affect the overall stability of devices. PVK will be irreversibly decomposed to PbI_2 and MAI at high temperatures. In order to further explore the effect of adding LDHs on the thermal stability of the devices, the thermal stability of PSCs with LDHs and control PSCs was tested under the conditions of relative humidity of 20–30% and temperature of 85°C. The results showed that PSCs with LDHs had better thermal stability than the control PSCs. As confirmed by the normalized efficiency loss, the PSCs with LDHs still maintained 58% of the original efficiency at 140 h, while the control PSCs decreased to 39% of the original efficiency (Fig. 1c). The color change of the corresponding PVK films at different times can demonstrate this phenomenon more visually (Fig. S3). Compared with the PVK films, the color of the PVK films with LDHs (FTO/TiO_2/PVK/LDHs) slowly

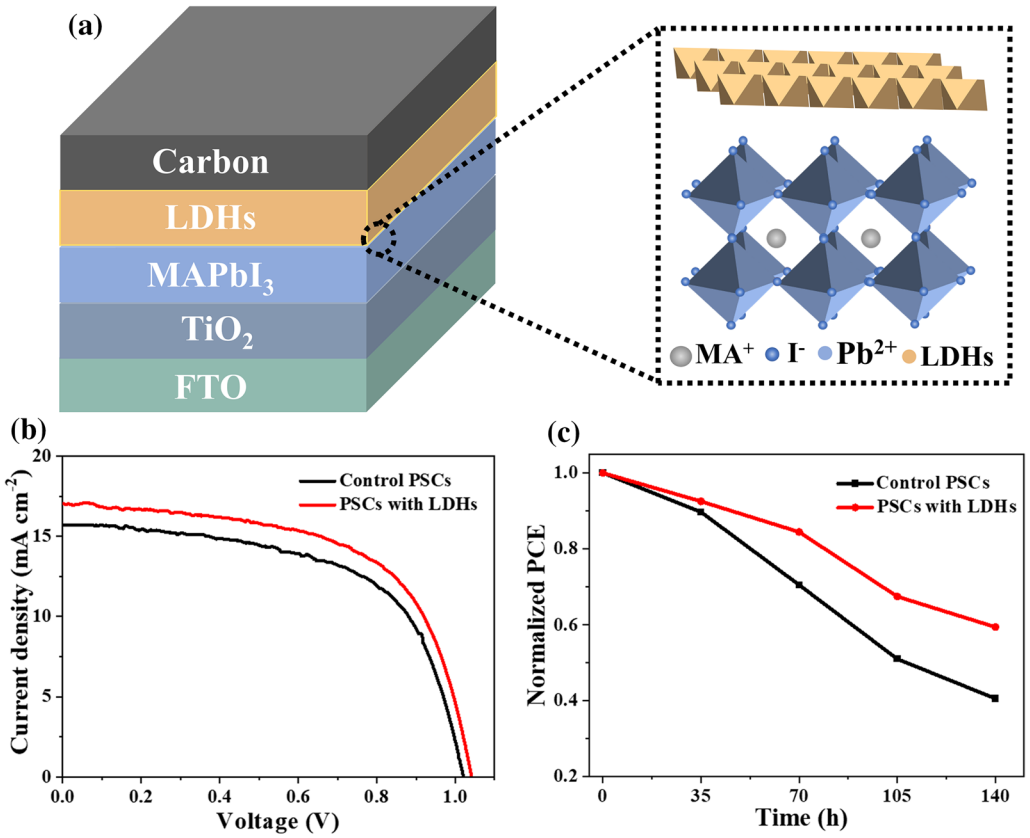

Fig. 1 (a) The PSC structure. (b) *J*–*V* characteristics. (c) Thermal stability measured at 85°C of the PSCs with LDHs and control PSCs.

Table I Photovoltaic parameters of the best-performing control PSCs and PSCs with LDHs.

Samples	V_{OC} (V)	J_{SC} (mA cm^{-2})	FF (%)	PCE (%)
Control PSCs	1.02	15.71	59.89	9.60
PSCs with LDHs	1.04	17.00	60.49	10.70

changed from black to yellow, while the PVK films basically turned yellow at 105 h, indicating that the PVK had decomposed. The UV-Vis absorption spectra were used to unclose the reason. The PVK films and PVK films with LDHs were prepared and heat-treated at 85°C for 0 h, 35 h, 70 h and 105 h, respectively, and the corresponding UV-Vis absorption spectra are shown in Fig. S4. The absorption intensity of the PVK films decreased significantly above 450 nm with the increase of storage time, probably due to the decomposition of PVK. In contrast, the UV-Vis spectra of the LDHs-modified PVK films showed less change in absorption intensity during the same storage time. The above results indicate that the PSCs with LDHs have better thermal stability.

The Performance Improvement Mechanism of PSCs with LDHs

Interaction Between LDH and PVK Layer

To confirm the interaction between the LDHs and the PVK layer, the FTIR spectra of LDHs, PVK films and PVK/LDHs films were compared and analyzed Fig. 2a. LDH has a strong absorption peak at 3450.03 cm^{-1}, corresponding to the stretching vibration of -OH. However, the stretching vibration peak of –OH in PVK/LDHs film moved to 3432.67 cm^{-1}, which indicated the interaction of –OH in LDHs with PVK layer. Figure 2b and Fig. S5 are the XPS spectra of the PVK film and PVK/LDHs film. The binding energies of Pb $4f_{7/2}$ and $4f_{5/2}$ peaks of the PVK films were 138.5 eV and 143.3 eV, respectively, and after modifying the PVK layer with LDHs, the binding energies shifted slightly to a higher level at 138.7 eV and 143.5 eV. After the introduction of LDHs, the binding energies of I $3d_{5/2}$ and $3d_{3/2}$ peaks also moved from 618.4 eV to 629.9 eV and 618.7 eV to 630.2 eV, respectively, suggesting interaction between LDHs and Pb^{2+} and I^-. The existence of the interaction between LDHs and PVK layer can be confirmed by FTIR and XPS spectra.

Energy Level Matching

CV measurements (Fig. 3a and b) were performed to investigate the electrochemical properties of LDHs. The highest occupied molecular orbital (HOMO) and lowest unoccupied molecular orbital (LUMO) energy levels of LDHs based on CV data were –5.0 eV and –2.9 eV, respectively, and the results were summarized in Table S1. The energy level diagram of PSC device was shown in Fig. 3c, and the energy levels of FTO, TiO_2, $MAPbI_2$ and carbon electrode are derived from previous work.[36,37] The HOMO energy level of LDHs is deeper than the valence band (VB, –5.4 eV) of PVK layer, so the holes generated in PVK can be effectively extracted. In addition, the LUMO energy level of LDHs is higher than the conduction band (CB, –3.9 eV) of the PVK layer, which can block the transport of electrons from the PVK layer to the carbon electrode, thus effectively preventing carrier recombination. Therefore, the energy levels of LDHs as HTL match the energy bands of PVK very well.

Hole Extraction

The PL and TRPL spectra of PVK film and PVK/LDHs film were measured to study the hole-extraction properties of LDHs as the HTL. As can be seen from Fig. 4a, PL intensity of the PVK/LDHs film was obviously lower than that of the PVK film, indicating that the charge can be transferred from PVK to LDHs, which confirmed the hole-extraction capability of LDHs. The carrier lifetime (τ) of PVK film and PVK/LDHs film were further compared by TRPL spectroscopy (Fig. 4b). The TRRL decay curves were fitted by the biexponential decay function:[38–40]

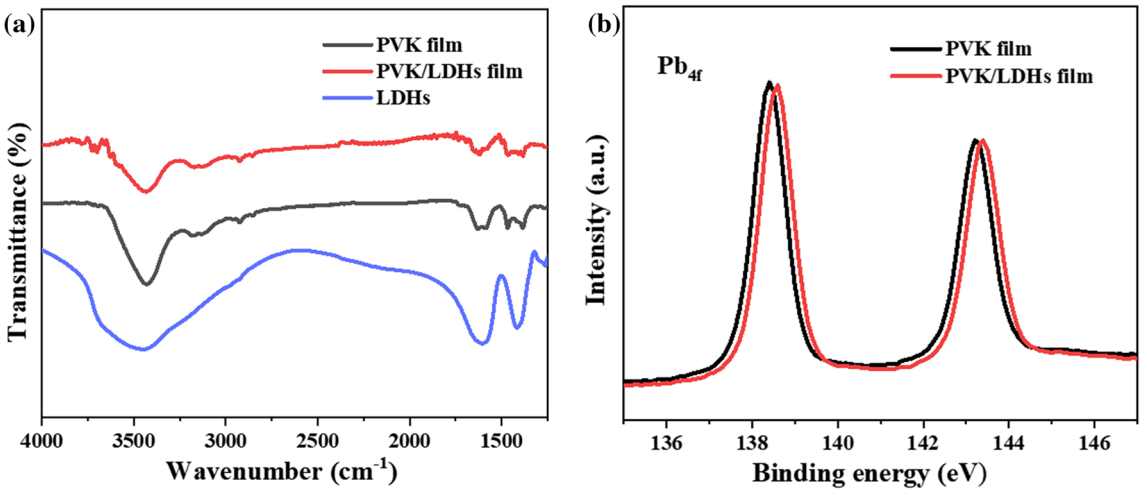

Fig. 2 (a) FTIR spectra of LDHs, PVK film and PVK/LDH film. (b) XPS spectra of Pb_{4f} peaks of PVK film and PVK/LDH film.

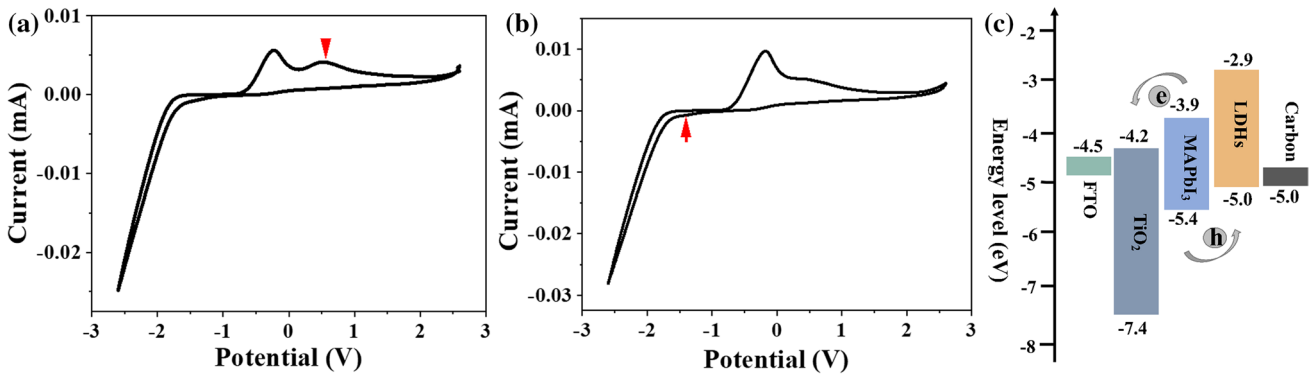

Fig. 3 The cyclic voltammogram curves of LDHs: (a) the positive scanning and (b) the negative scanning. (c) Energy diagram of each layer of PSCs.

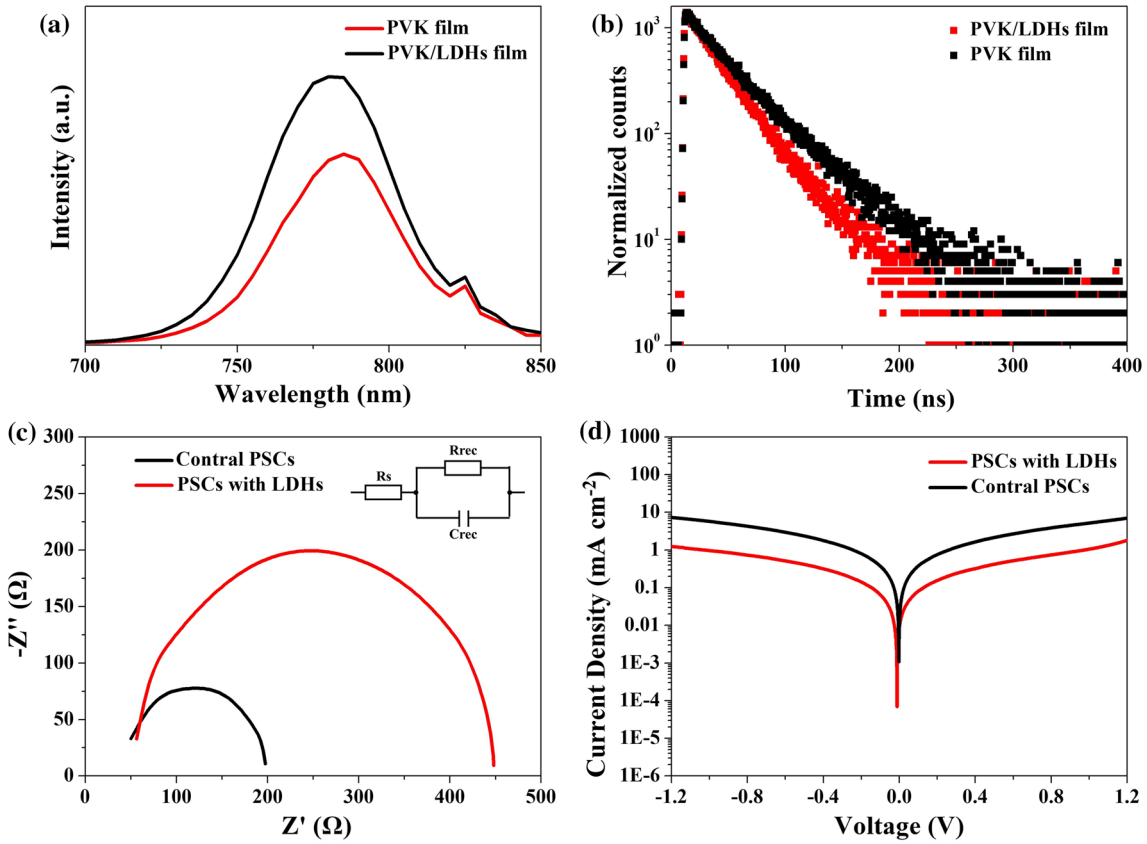

Fig. 4 (a) Steady-state and (b) time-resolved PL spectra of the PVK films and PVK/LDHs films. (c) EIS measurement results. (d) Dark *J*–*V* curves of control PSCs and PSCs with LDHs.

$$F(\mathrm{t}) = \mathrm{A}_1 \exp\left(-\frac{t}{\tau_1}\right) + \mathrm{A}_2 \exp\left(-\frac{t}{\tau_2}\right) \quad (3)$$

where τ_1 and τ_2 are the fast decay component and the slow decay component, respectively, and they relate to the non-radiative recombination and radiative recombination. The average carrier lifetimes are calculated by the formula:[41]

$$\tau_{\mathrm{avg}} = \frac{\mathrm{A}_1 {\tau_1}^2 + \mathrm{A}_2 {\tau_2}^2}{\mathrm{A}_1 \tau_1 + \mathrm{A}_2 \tau_2} \quad (4)$$

the corresponding fitting parameters were listed in Table S2. The lifetimes of PVK film and PVK/LDHs film were 41.99 and 29.10 ns, respectively. Obviously, the PL lifetime of PVK film was reduced due to the deposition of LDHs. The shorter lifetime of PVK/LDHs film indicated the addition of LDHs promotes hole transfer and extraction.

In order to further explore the process of charge transport and recombination after adding LDH as HTL, the EIS spectra and dark *J*–*V* characteristics measurements were performed on control PSCs and PSCs with LDHs. The EIS spectra were shown in Fig. 3c, and the fitted parameters of series resistance (R_s) and charge transfer resistance (R_{rec}) were listed in Table S3. The R_{rec} of PSCs with LDHs is 394.6 Ω, which is higher than that of control PSC (155.6 Ω), indicating rapid charge transfer and effective inhibition of charge recombination. The dark *J*–*V* curves of control PSCs and PSCs with LDHs were shown in Fig. 3d. The leakage current of PSCs with LDHs is lower than that of control PSCs, implying that adding LDHs as HTL in PSC can reduce the current leakage, which can help to improve the device efficiency.

Morphology and Structure Effect

Since the quality of the PVK film has great influence on PSC device performance, XRD, SEM and AFM measurements were performed to investigate the film. The structures of PVK film and PVK/LDHs film were compared by XRD patterns (Fig. S6). The diffraction peak at 14.2° corresponding to the (110) plane of the PVK lattice shows remarkable enhancement after the addition of LDHs, suggesting the higher crystallinity and the enhanced stability of the PVK crystals. SEM images of the PVK film and PVK/LDHs film are shown in Fig. 5a and b. After the deposition of LDHs, the PVK/LDHs film exhibited dense morphology, large grain

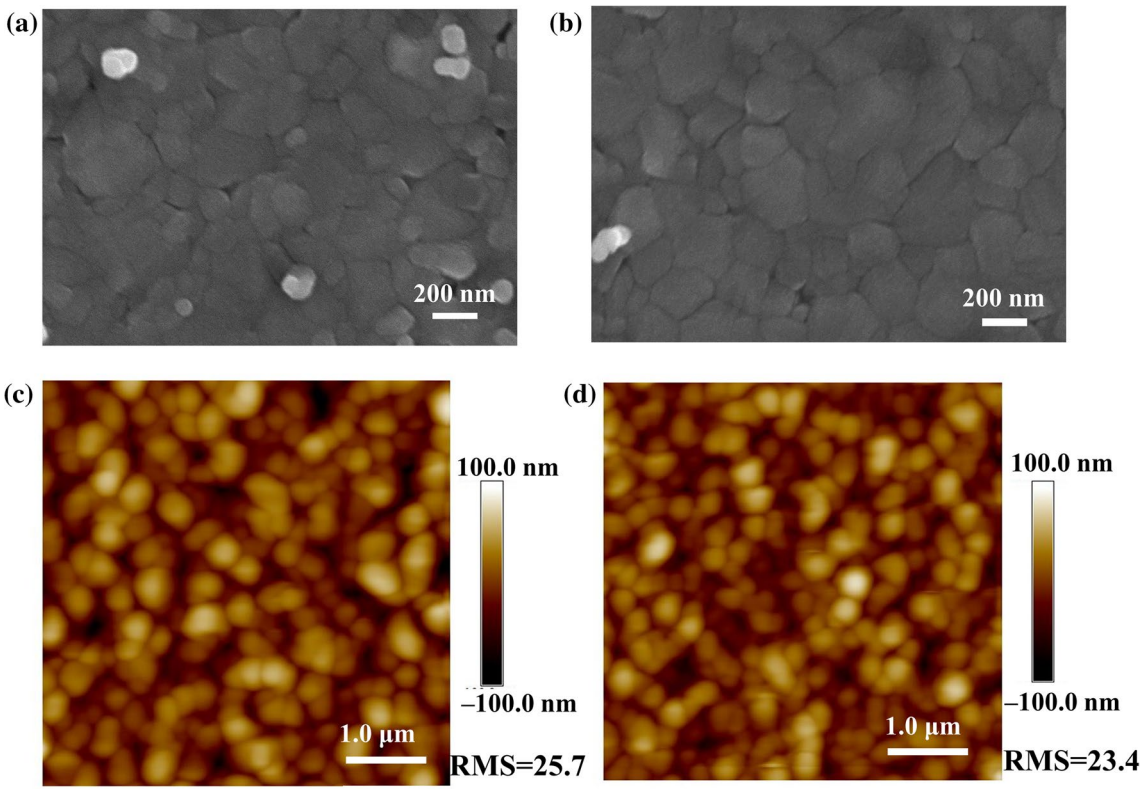

Fig. 5 Top-view SEM images of (a) PVK film and (b) PVK/LDHs film. AFM images of (c) PVK film and (d) PVK/LDHs film.

size and reduced pinholes. The AFM images in Fig. 5c and d showed that the root mean square (RMS) roughness of pristine PVK film is 25.7 nm, while the RMS roughness of the PVK/LDHs film reduce to 23.4 nm, suggesting that the PVK film coated with LDHs becomes much smoother, which contributes to better contact with the carbon electrode and improves the stability of the device.

Conclusions

In summary, inorganic LDH nanoparticles were applied in PSC devices as an HTL. Mechanistic studies showed that the valence band of the LDH matches the valence band of the PVK, which can transport holes well. Meanwhile, LDH limits the movement of electrons to the anode, thus reducing carrier recombination. In addition, LDH has surface hydroxyl groups, which can combine with uncoordinated Pb^{2+} to fill the holes in PVK layer, thus improving the fill factor of PSC devices. LDH can be used as a protective layer, preventing the PVK layer from decomposing in contact with oxygen and heat, consequently enhancing device stability. We used LDHs instead of expensive organic HTL, overcoming the problems of high cost and poor stability. Therefore, LDH is expected to be a potential candidate for HTL, and this study provides a simple strategy for fabricating low-cost and stable PSC.

Supplementary Information The online version contains supplementary material available at https://doi.org/10.1007/s11664-023-10750-x.

Acknowledgments This work was supported by the National Natural Science Foundation of China (22171018), the Fundamental Research Funds for the Central Universities (12060093063), and the Experiments for Space Exploration Program and the Qian Xuesen Laboratory, China Academy of Space Technology (TKTSPY-2020-02-04).

Conflict of interest The authors declare that they have no conflict of interest.

References

1. D.H. Kim, J.B. Whitaker, Z. Li, M.F.A.M. van Hest, and K. Zhu, Outlook and challenges of perovskite solar cells toward terawatt-scale photovoltaic module technology. *Joule* 2, 1437 (2018).
2. P.-K. Kung, M.-H. Li, P.-Y. Lin, Y.-H. Chiang, C.-R. Chan, T.-F. Guo, and P. Chen, A review of inorganic hole transport materials for perovskite solar cells. *Adv. Mater. Interfaces* 5, 1800882 (2018).
3. N.J. Jeon, J.H. Noh, W.S. Yang, Y.C. Kim, S. Ryu, J. Seo, and S.I. Seok, Compositional engineering of perovskite materials for high-performance solar cells. *Nature* 517, 476 (2015).

4. D.G. Lee, D.H. Kim, J.M. Lee, B.J. Kim, J.Y. Kim, S.S. Shin, and H.S. Jung, High efficiency perovskite solar cells exceeding 22% via a photo-assisted two-step sequential deposition. *Adv. Funct. Mater.* 31, 2006718 (2021).
5. K. Wang, C. Wu, Y. Hou, D. Yang, T. Ye, J. Yoon, M. Sanghadasa, and S. Priya, Isothermally crystallized perovskites at room-temperature. *Energy Environ. Sci.* 13, 3412 (2020).
6. A. Kojima, K. Teshima, Y. Shirai, and T. Miyasaka, Organometal halide perovskites as visible-light sensitizers for photovoltaic cells. *J. Am. Chem. Soc.* 131, 6050 (2009).
7. H. Min, D.Y. Lee, J. Kim, G. Kim, K.S. Lee, J. Kim, M.J. Paik, Y.K. Kim, K.S. Kim, M.G. Kim, T.J. Shin, and S.I.L. Seok, Perovskite solar cells with atomically coherent interlayers on SnO_2 electrodes. *Nature* 598, 444–450 (2021).
8. Z. Yu and L. Sun, Recent progress on hole-transporting materials for emerging organometal halide perovskite solar cells. *Adv. Energy Mater.* 5, 1500213 (2015).
9. Z.H. Bakr, Q. Wali, A. Fakharuddin, L. Schmidt-Mende, T.M. Brown, and R. Jose, Advances in hole transport materials engineering for stable and efficient perovskite solar cells. *Nano Energy* 34, 271 (2017).
10. Z. Yu and L. Sun, Inorganic hole-transporting materials for perovskite solar cells. *Small Methods* 2, 1700280 (2018).
11. D. Zhang, P. Xu, T. Wu, Y. Ou, X. Yang, A. Sun, B. Cui, H. Sun, and Y. Hua, Cyclopenta hi aceanthrylene-based dopant-free hole-transport material for organic-inorganic hybrid and all-inorganic perovskite solar cells. *J. Mater. Chem. A* 7, 5221 (2019).
12. F.M. Rombach, S.A. Haque, and T.J. Macdonald, Lessons learned from spiro-OMeTAD and PTAA in perovskite solar cells. *Energy Environ. Sci.* 14, 5161 (2021).
13. S. Akin, Y. Liu, M.I. Dar, S.M. Zakeeruddin, M. Gratzel, S. Turan, and S. Sonmezoglu, Hydrothermally processed $CuCrO_2$ nanoparticles as an inorganic hole transporting material for low-cost perovskite solar cells with superior stability. *J. Mater. Chem. A* 6, 20327 (2018).
14. X. Li, D. Bi, C. Yi, J.-D. Decoppet, J. Luo, S.M. Zakeeruddin, A. Hagfeldt, and M. Gratzel, A vacuum flash-assisted solution process for high-efficiency large-area perovskite solar cells. *Science* 353, 58 (2016).
15. H.W. Qiao, S. Yang, Y. Wang, X. Chen, T.Y. Wen, L.J. Tang, Q. Cheng, Y. Hou, H. Zhao, and H.G. Yang, A gradient heterostructure based on tolerance factor in high-performance perovskite solar cells with 0.84 fill factor. *Adv. Mater.* 31, 1804217 (2019).
16. T.Y. Wen, S. Yang, P.F. Liu, L.J. Tang, H.W. Qiao, X. Chen, X.H. Yang, Y. Hou, and H.G. Yang, Surface electronic modification of perovskite thin film with water-resistant electron delocalized molecules for stable and efficient photovoltaics. *Adv. Energy Mater.* 8, 1703143 (2018).
17. H.H. Park, Efficient and stable perovskite solar cells based on inorganic hole transport materials. *Nanomaterials* 12, 112 (2022).
18. Z. Hawash, L.K. Ono, S.R. Raga, M.V. Lee, and Y. Qi, Air-exposure induced dopant redistribution and energy level shifts in spin-coated spiro-meotad films. *Chem. Mater.* 27, 562 (2015).
19. A.K. Jena, Y. Numata, M. Ikegami, and T. Miyasaka, Role of spiro-OMeTAD in performance deterioration of perovskite solar cells at high temperature and reuse of the perovskite films to avoid Pb-waste. *J. Mater. Chem. A* 6, 2219 (2018).
20. J. Shi, B. Li, Q. Zhang, and Y. Rui, Electrodeposited ternary $AgCuO_2$ nanocrystalline films as hole transport layers for inverted perovskite solar cells. *J. Alloys Compd.* 890, 161879 (2022).
21. B. Gil, A.J. Yun, Y. Lee, J. Kim, B. Lee, and B. Park, Recent progress in inorganic hole transport materials for efficient and stable perovskite solar cells. *Electron. Mater. Lett.* 15, 505 (2019).
22. S. Bellani, A. Bartolotta, A. Agresti, G. Calogero, G. Grancini, A. Di Carlo, E. Kymakis, and F. Bonaccorso, Solution-processed two-dimensional materials for next-generation photovoltaics. *Chem. Soc. Rev.* 50, 11870 (2021).
23. U.K. Aryal, M. Ahmadpour, V. Turkovic, H.-G. Rubahn, A. Di Carlo, and M. Madsen, 2D materials for organic and perovskite photovoltaics. *Nano Energy* 94, 106833 (2022).
24. J. Yu, Q. Wang, D. O'Hare, and L. Sun, Preparation of two dimensional layered double hydroxide nanosheets and their applications. *Chem. Soc. Rev.* 46, 5950 (2017).
25. S. Argote-Fuentes, R. Feria-Reyes, E. Ramos-Ramirez, N. Gutierrez-Ortega, and G. Cruz-Jimenez, Photoelectrocatalytic degradation of congo red dye with activated hydrotalcites and copper anode. *Catalysts* 11, 211 (2021).
26. L. Pan, H. Huang, and M. Niederberger, Layered cobalt hydrotalcite as an advanced lithium-ion anode material with high capacity and rate capability. *J. Mater. Chem. A* 7, 21264 (2019).
27. Q. Liu, X. Chen, W. Hu, M. Zhang, L. Ding, M. Wang, Q. Qiao, and S. Yang, Beyond metal oxides: introducing low-temperature solution-processed ultrathin layered double hydroxide nanosheets into polymer solar cells toward improved electron transport. *Solar Rrl* 3, 1800299 (2019).
28. V. Truong-Giang, Y. Tai, and C.-Y. Chiang, Multifunctional ternary hydrotalcite-like nanosheet arrays as an efficient Co-catalyst for vastly improved water splitting performance on bismuth vanadate photoanode. *J. Catal.* 370, 1 (2019).
29. L. Teruel, Y. Bouizi, P. Atienzar, V. Fornes, and H. Garcia, Hydrotalcites of zinc and titanium as precursors of finely dispersed mixed oxide semiconductors for dye-sensitized solar cells. *Energy Environ. Sci.* 3, 154 (2010).
30. Z. Li, M. Shao, H. An, Z. Wang, S. Xu, M. Wei, D.G. Evans, and X. Duan, Fast electrosynthesis of Fe-containing layered double hydroxide arrays toward highly efficient electrocatalytic oxidation reactions. *Chem. Sci.* 6, 6624 (2015).
31. S. Mancipe, J.J. Martinez, C. Pinzon, H. Rojas, D. Solis, and R. Gomez, Effective photocatalytic degradation of Rhodamine B Using tin semiconductors over hydrotalcite-type materials under sunlight driven. *Catal. Today* 372, 191 (2021).
32. L. Kong, K. Liang, R. Wang, J. Liu, W. Shi, and C. Lu, Anisotropy growth of perovskite crystal induced by layered double hydroxide for efficiency enhancement of solar cell. *Electrochim. Acta* 438, 141586 (2023).
33. Q. Lin, Z. Wang, H.J. Snaith, M.B. Johnston, and L.M. Herz, Hybrid perovskites: prospects for concentrator solar cells. *Adv. Sci.* 5, 1700792 (2018).
34. S.O.A. Ahmad, A. Ashfaq, M.U. Akbar, M. Ikram, K. Khan, F. Wang, M. Ikram, and A. Mahmood, Application of two-dimensional materials in perovskite solar cells: recent progress, challenges, and prospective solutions. *J. Mater. Chem. C* 9, 14065 (2021).
35. M.I. Hossain, A.M. Saleque, S. Ahmed, I. Saidjafarzoda, M. Shahiduzzaman, W. Qarony, D. Knipp, N. Biyikli, and Y.H. Tsang, Perovskite/perovskite planar tandem solar cells: a comprehensive guideline for reaching energy conversion efficiency beyond 30%. *Nano Energy* 79, 105400 (2021).
36. F. Hao, C.C. Stoumpos, R.P.H. Chang, and M.G. Kanatzidis, Anomalous band gap behavior in mixed Sn and Pb perovskites enables broadening of absorption spectrum in solar cells. *J. Am. Chem. Soc.* 136, 8094 (2014).
37. H. Chen, and S. Yang, Carbon-based perovskite solar cells without hole transport materials: the front runner to the market? *Adv. Mater.* 29, 1603994 (2017).
38. R. Chen, Y. Feng, C. Zhang, M. Wang, L. Jing, C. Ma, J. Bian, and Y. Shi, Carbon-based HTL-Free modular perovskite solar cells with improved contact at perovskite/carbon interfaces. *J. Mater. Chem. C* 8, 9262 (2020).
39. C. Hanmandlu, S. Swamy, A. Shing, H.-A. Chen, C.-C. Liu, C.-S. Lai, A. Mohapatra, C.-W. Pao, P. Chen, and C.-W. Chu,

Suppression of surface defects to achieve hysteresis-free inverted perovskite solar cells via quantum dot passivation. *J. Mater. Chem. A* 8, 5263 (2020).
40. C. Wu, K. Wang, Y. Jiang, D. Yang, Y. Hou, T. Ye, C.S. Han, B. Chi, L. Zhao, S. Wang, W. Deng, and S. Priya, All electrospray printing of carbon-based cost-effective perovskite solar cells. *Adv. Funct. Mater.* 31, 2006803 (2021).
41. D. Xin, S. Tie, R. Yuan, X. Zheng, J. Zhu, and W.-H. Zhang, Defect passivation in hybrid perovskite solar cells by tailoring the electron density distribution in passivation molecules. *ACS Appl. Mater. Interfaces* 11, 44233 (2019).